J Mater Sci (2007) 42:7263–7274
DOI 10.1007/s10853-006-1460-2

The derivation of the microfibril angle in softwood using wide-angle synchrotron X-ray diffraction on structurally characterised specimens

Kenneth M. Entwistle · K. Kong · M. A. MacDonald · N. Navaranjan · S. J. Eichhorn

Received: 20 September 2006 / Accepted: 15 December 2006 / Published online: 10 May 2007

Abstract The micro-fibril angle of specimens of *Pinus radiata* was measured by preparing a microsection of 1000 wood cell walls and irradiating with an X-ray beam from a synchrotron source. The (002) X-ray intensity scattered by the cellulose fibres in each wall was calculated, and the total azimuthal distribution was determined by summing the individual intensities. This is compared to the predicted intensity distributions obtained from geometrical measurements on images of real wood cell walls. The length and orientation of each of the wood cells was prepared, and based on these measurements the predicted intensity distribution was determined. It is shown that an analysis derived for square wood cells is sufficient for the accurate determination of microfibril angle, which an assumption that has not been previously verified.

Introduction

X-ray scattering from wood specimens has been reported extensively in the past. Wide-angle X-ray measurements of the microfibril angle in the S2 layers of softwood were pioneered by Cave [1] and by Meylan [2]. Later studies attempted to derive the microfibril angle as a function of anatomical features, such as in the earlywood and latewood regions of eucalypt species [3]. In fact this technique was chosen for measurements using the Silviscan^{TM} equipment [4]. The theory for diffraction from wood cell walls has also been well-established by Cave [5, 6].

In recent years a number of papers have been published by Fratzl and co-workers [7, 8] on the use of microfocus X-ray diffraction using a synchrotron source for local characterisation of the fibril angle in wood. In particular, a study of the change in the fibril angle with deformation of a small number of wood cell walls, in the form of a 'foil' of material, has also been reported [9]. Another more recent study by [10] has shown some anomalous behaviour of the microfibril angle during deformation, wherein a decrease in the absolute value is seen during the strain-hardening region of the macrodeformation of the material. Finally, the determination of the microfibril angle of wood has also been recently extensively reviewed and placed in a biological context by Barnett and Bonham [11].

In a previous paper [12] the cellulose microfibril angles of softwood specimens of *Pinus sylvestris* were measured using Small-Angle X-ray Scattering (SAXS). The length and orientation of about 1000 cell walls was measured by quantitative image analysis, and the scattered intensity distribution round a circle centred on the unscattered beam was calculated and compared to the measured intensity. These 1000 cells were thought to be representative of a realistic volume of wood for bulk material properties. Values of the microfibril angle M and the standard deviation of the normal distribution of intensity from a single fibre σ_{φ} were adjusted to achieve the best fit between the experimental and the calculated distributions. The procedure was carried out on six specimens cut from the same

K. M. Entwistle (✉) · K. Kong · S. J. Eichhorn
Materials Science Centre, School of Materials,
University of Manchester, Grosvenor Street, Manchester,
M1 7HS, UK
e-mail: ken.entwistle@manchester.ac.uk

M. A. MacDonald
CCLRC Daresbury Laboratory, Warrington,
Cheshire WA4 4AD, UK

N. Navaranjan
Ensis Papro, Rotorua, New Zealand

growth ring and oriented so that the radial plane lay at differing angles to the irradiated front face of the specimen.

Here we present the results of a similar and complementary investigation using wide-angle X-ray scattering. The main purpose of the work is to test the assumption of the validity of the analysis of fibril angle based on square cells. This is done by taking into account the real cell structure of the material from image analysis measurements, and comparing theoretical scattering of this structure against what is seen in reality.

A previous investigation [13] compared the calculated and the measured azimuth angle at peak intensity from structurally characterised specimens which were irradiated at 45° to the radial direction. In the present work the calculated intensity is fitted to the whole of the intensity distribution round the (002) circle, which was not done in the previous investigation. The present work also uses a wider range of angles of irradiation orientation by carefully sectioning samples at various angles to the radial direction. The interpretation of the distribution of intensity round the (002) diffraction circle commonly assumes, either overtly or by implication, that all the cell walls are oriented in either the radial or in the tangential directions and hence we also test this assumption through this analysis.

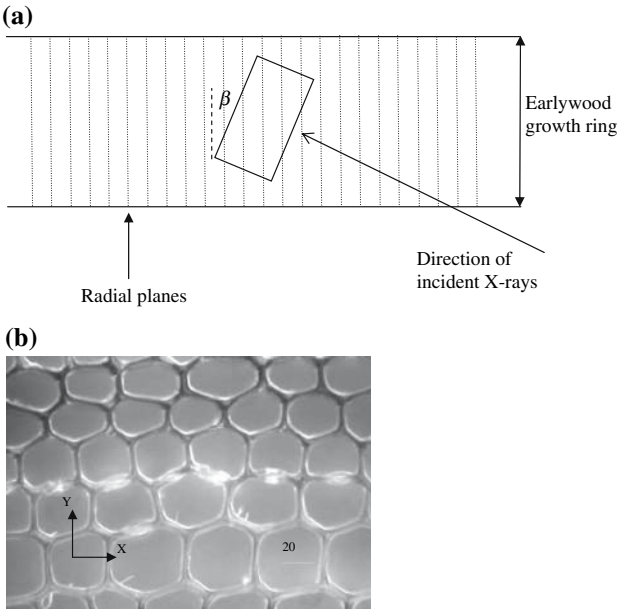

Fig. 1 (**a**)The approximate relative location of a specimen cross-section in a growth ring and the direction of the diffracting X-ray beam and (**b**) an optical image of part of the microstructure used to measure the length and orientation of the cell walls. The *x*-axis lies in the radial direction. The scale bar unit is microns

Experimental

Specimens 10 × 2 × 1 mm were cut from one early growth ring of *Pinus radiata*. In all, eight specimens were extracted. Each specimen had the longitudinal direction parallel to the cell axis, but the cross-section was oriented so that the 2 mm wide face, which was the face on which the X-rays were normally incident, lay at different angles β to the radial direction. The geometry of the sections is schematically illustrated in Fig. 1a. The prepared values of β were 0°, 12°, 22°, 37°, 44°, 50°, 53° and 63°. In these specimens, all the (002) diffracted beams from a particular cell wall passed through identical distances in the wood and were therefore equally absorbed.

A section was prepared in the radial-tangential plane which revealed the cross-section of the cell structure. The length and the orientation of about 1,000 cell walls were measured using a Scion image analyser. An image of a micro-section of one of the wood samples is shown in Fig. 1b. A two-dimensional rectangular coordinate system was set up with the *x*-axis in the radial direction and the *y*-axis in the transverse direction. The coordinates of the two ends of a cell wall (x_i, y_i) and (x_j,y_j) were determined and the length of the wall was calculated using the equation

$$\Delta L_{ij} = \sqrt{(x_j - x_i)^2 + (y_j - y_i)^2} \quad (1)$$

The orientation (θ) of the wall relative to the *x*-direction (radial) was derived using the expression

$$\theta = \arctan \frac{(y_j - y_i)}{(x_j - x_i)} \quad (2)$$

where anti-clockwise rotations relative to the radial direction were defined to be positive. The total cell wall length in each 1° range was collected and this length was plotted against the mean value of θ. These data are plotted in Fig. 2. The length of the radial walls (θ = ± 45°) was 1.8 times that of the tangential walls.

Station 14.1 of the Daresbury Synchrotron Light Source (SLS) was used to obtain wide angle X-ray diffraction 2D patterns of the wood specimens, examples of which are shown in Fig. 3. An X-ray wavelength of 0.15 nm, a specimen to detector (Quantum 4 ADSC detector with pixel sizes of 81.6 μm^2) distance of 83 cm and an exposure time of 60 s was used to obtain the patterns. Each specimen was mounted in a square picture-frame holder just ahead of the beam stop with its 2 mm wide flat face perpendicular to the beam direction. Analysis of each pattern, using the FIT2D software [14, 15], involved obtaining a radial intensity profile around the (002) diffraction circle using a radial distance of 80 (arbitrary units). Each profile was then fitted using mixed Gaussian/Lorentzian functions and an algorithm based on work by Marquardt [16] within the

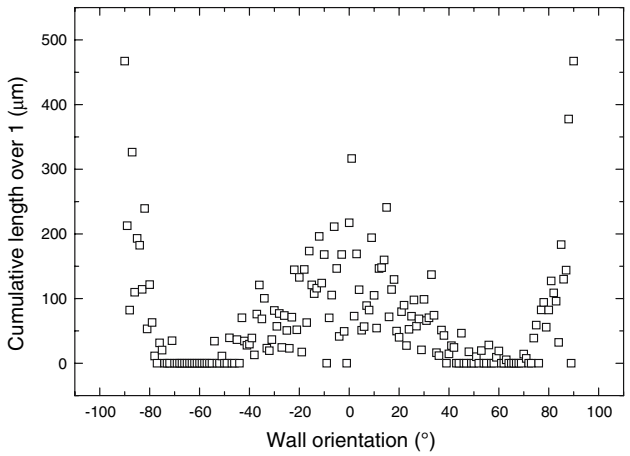

Fig. 2 The total length of cell wall in a 1° range and its orientation relative to the radial direction

GRAMS-32 spectral analysis software, and peak intensities and widths were obtained for further analysis.

Calculation of the relation between the azimuthal angle of the diffractions and the cell wall orientation

The basic analysis of the wide-angle X-ray diffraction from a cellulose fibre lying at an arbitrary orientation relative to the X-ray beam has been previously reported [17]. Figure 4 shows a cell wall with two S2 layers from contiguous cells. This structure has two sets of cellulose microfibrils lying symmetrically at the microfibril angle M to the cell axis which is vertical. The normal to the cell wall lies at an angle α to the incident X-ray beam, where α is positive in the anti-clockwise direction. The two sets of cellulose microfibrils, one from each S2 layer, are indicated and designated f1 and f2. Each set generates two (002) diffraction spots so there are four spots on the (002) circle. The spots from each fibril are indicated by shading that matches the shading of the fibril. It will be noted that the two spots from one fibril are not generally diametrically opposite.

We designate the spots on the right-hand side of the polar line 1R and 2R from the fibrils f1 and f2 respectively, and correspondingly 1L and 2L on the left-hand side. If the wall is irradiated with X-rays of wavelength 0.15 nm then this will give a corresponding Bragg angle γ of 11.5°. The azimuth angles for the spots are positive if they lie above the equator of the diffraction circle. The variation of the azimuth angle φ for each of the four spots as a function of the cell wall orientation α is given by four equations. Although the general structure of these equations is well known, care is needed to establish that the signs are those appropriate to the sign conventions adopted for the four angles involved. For this reason the four relevant equations are given as

$$\cot M \sin \varphi_{1R} = \sin \alpha \tan \gamma - \cos \alpha \cos \varphi_{1R} \quad (3)$$

$$\cot M \sin \varphi_{2R} = -(\sin \alpha \tan \gamma - \cos \alpha \cos \varphi_{2R}) \quad (4)$$

$$\cot M \sin \varphi_{1L} = \sin \alpha \tan \gamma + \cos \alpha \cos \varphi_{1L} \quad (5)$$

$$\cot M \sin \varphi_{2L} = -(\sin \alpha \tan \gamma + \cos \alpha \cos \varphi_{2L}) \quad (6)$$

for spots 1R, 2R, 1L and 2L respectively.

It is possible to extract from these conditions a set of relations that give values for the azimuthal angles as

$$\varphi_{1R} = 2 \arctan \left[\frac{\cot M - \sqrt{(\cot^2 M - (A - C)(A + C)}}{(A + C)} \right] \quad (7)$$

and

$$\varphi_{2R} = 2 \arctan \left[\frac{\sqrt{(\cot^2 M - (A - C)(A + C)} - \cot M}{(A + C)} \right] \quad (8)$$

for spots 1R and 2R respectively, where

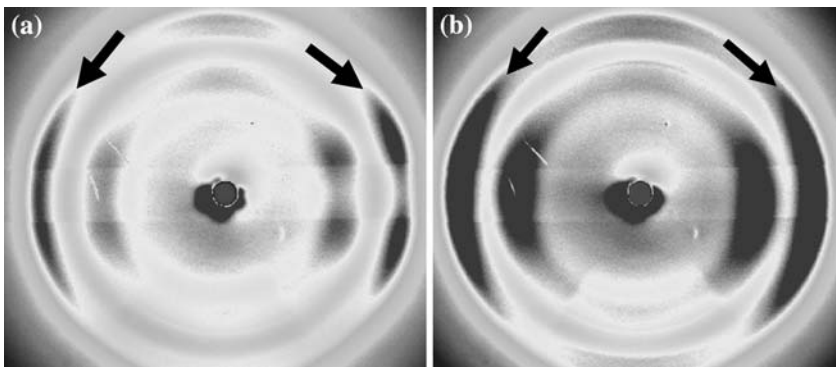

Fig. 3 A typical wide angle X-ray diffraction pattern showing the presence of the (002) circle (arrows)

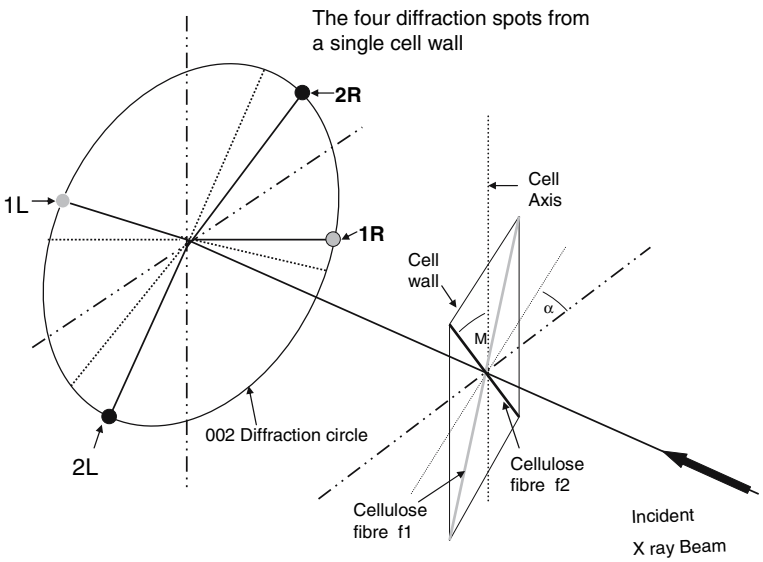

Fig. 4 Diagram showing the cell wall with two S2 layers and two sets of microfibrils f1 and f2. The normal to the cell wall lies at an angle α to the incident X-ray beam. There are four (002) diffraction spots, two from each microfibril, 1R and 1L are from f1 and 2R and 2L are from f2

$$A = \sin\alpha \tan\gamma \tag{9}$$

and

$$C = \cos\alpha \tag{10}$$

Hence, φ_{1R} and φ_{2R} lie symmetrically astride the equator. For spots 1L and 2L the following equations apply for their respective azimuthal angles

$$\varphi_{1L} = 2\arctan\left[\frac{\cot M - \sqrt{(\cot^2 M - (A-C)(A+C)}}{(A-C)}\right] \tag{11}$$

$$\varphi_{2L} = 2\arctan\left[\frac{\sqrt{(\cot^2 M - (A-C)(A+C)} - \cot M}{(A-C)}\right] \tag{12}$$

So, φ_{1L} and φ_{2L} are also symmetrically located astride the equator. However, the two spots from a single fibril, for example 1R and 1L, are not in general diametrically opposite. The curves in Fig. 5 (continuous lines) show the variation of the azimuth angle with cell wall orientation for the four spots derived from Eqs. 7–12. A microfibril angle of 30° was used to determine these curves.

An optical analogue for the (002) diffraction by a cellulose fibre

It is possible to devise an optical analogy which will reproduce the azimuth angles of the X-ray diffraction spots as a function of the cell wall orientation. This serves to provide a check that the signs in Eqs. 7 to 12 are correct.

The diffracted beams arise from Bragg reflections from the (002) planes of the monoclinic unit cell. The normal to these planes is perpendicular to the fibril axis. With radiation of wavelength 0.15 nm, the Bragg angle is 11.5° so a Bragg reflection deflects the beam through 23°. If a mirror is used to represent an (002) plane then a laser beam directed at 11.5° to the plane of the mirror will simulate a Bragg reflection. A mirror is fixed to a rod which is cut away so that the reflecting face of the mirror lies along the rod axis, and so the normal to the reflecting surface is perpendicular to the rod axis. The rod represents a cellulose fibril. The rod is mounted in a goniometer which permits the rod to be rotated about its axis

The rod axis is set at any chosen angle to the vertical, representing the microfibril angle. The plane containing the rod axis and the vertical axis is the plane of the cell wall, since the vertical axis is the cell axis.

The system sits on a turntable which can be rotated through 360° about the vertical axis and permits the cell wall orientation α relative to the laser beam to be varied. A sketch of the arrangement is shown in Fig. 6.

A horizontal laser beam shines on the mirror and is reflected to a screen which the undeflected beam strikes at normal incidence. A circle is drawn on the screen corresponding to the intersection of a cone with its apex located at the point at which the beam strikes the mirror and of semi-angle 2γ = 23°. Any reflection from the mirror that lies on the circle satisfies the Bragg condition and therefore reproduces the position of the X-ray spot. The horizontal turntable was rotated through 360° in 10° steps to simulate variations in α. At each step the rod carrying the mirror was rotated about its axis to bring the reflected spot on to the (002) circle on the screen. The azimuth angle of this spot was recorded. At each value of α there are two mirror positions that satisfy the Bragg condition; one produces a

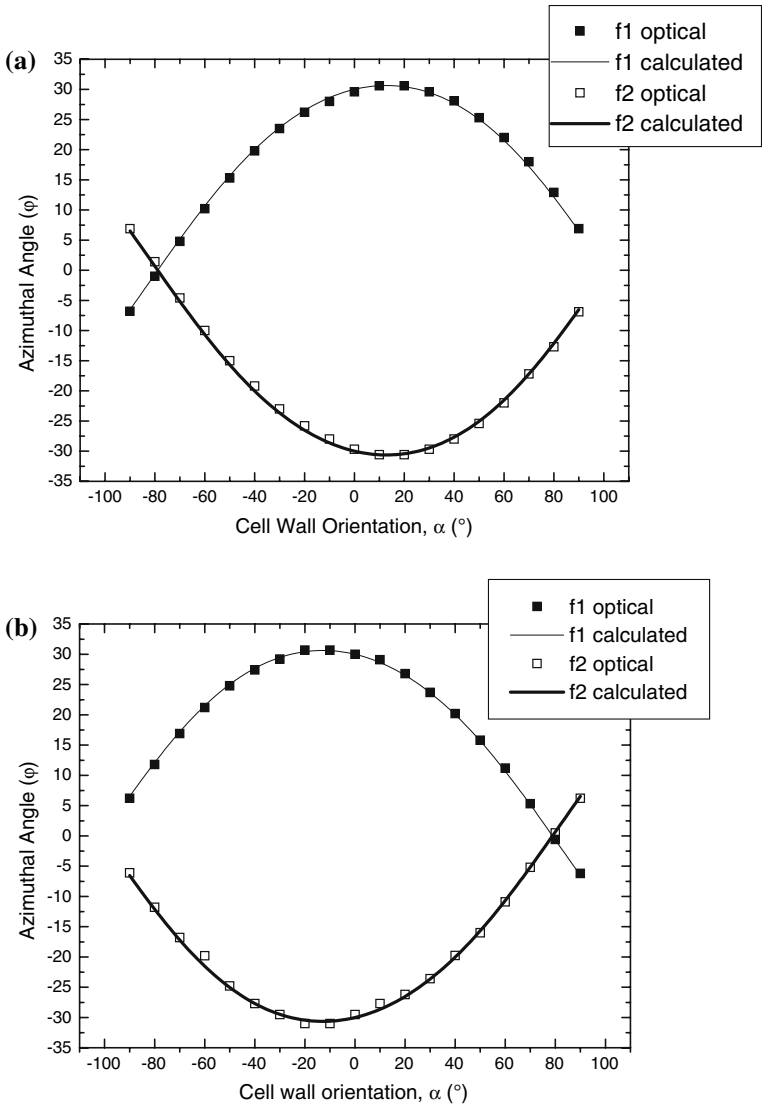

Fig. 5 The variation of azimuth angle φ with the cell wall orientation relative to the X-ray beam α where (**a**) are for the spots on the left hand side of the polar line and (**b**) is for the right hand spots. The continuous lines are the calculated values from Eqs. (5)–(10) and the points are the values determined from the optical analogue. The microfibril angle is assumed to be 30°

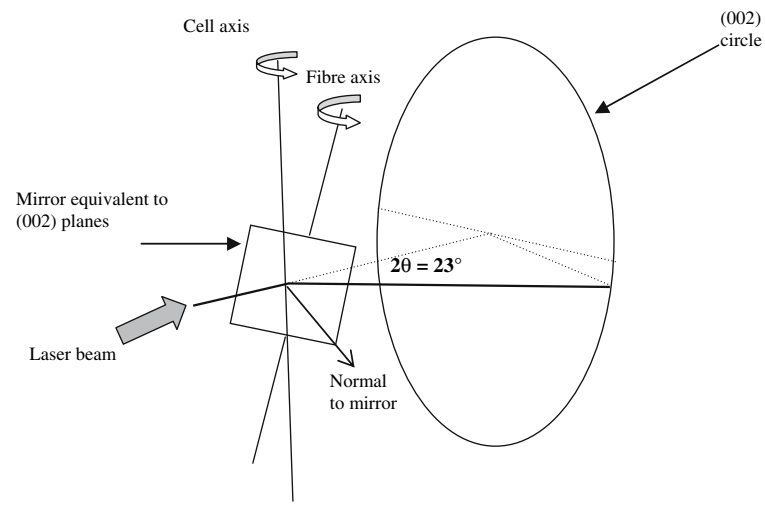

Fig. 6 An optical construction of the analogue of the X-ray diffraction from a cellulose fibril. The fibril is represented by the rod carrying a mirror which represents the (002) planes. When the laser beam strikes the mirror at an angle of 12°, the reflected beam falls on the (002) circle

spot on the right hand side of the polar line and the other on the left. All the azimuth angles determined optically are plotted in Fig. 5 together with the values calculated from Eqs. 7–12. The excellent agreement between the optically measured and the calculated vales confirms that Eqs. 7–12 are valid and can be used with confidence to interpret the X-ray data.

Calculation of the total scattered intensity

The total intensity distribution round the (002) circle was calculated by summing the intensity generated by each of the 180 one degree groups of cell walls represented in Fig. 2. For the specimen cut with $\beta = 0°$ the angle between the X-ray beam and the cell walls α is equal to θ and is given by Fig. 2 directly. The four azimuth angles for each cell wall are given by putting these values of α in Eqs. 7–12. Because the X-ray beam cross-section is rectangular, all the cells are irradiated along the same length in the axial direction of the cells. The diffracted intensity from a cell wall is proportional to the volume of cellulose fibres irradiated. This in turn is proportional to the irradiated cell wall volume. Since the all irradiated lengths are the same, the volume is proportional to the wall dimension in the radial/transverse plane—assuming that the cell wall thicknesses are all equal. The values of this wall dimension for all the cell walls, which are derived from image analysis of microsections like Fig. 1a, are collected in Fig. 2. The intensity generated by each diffraction is spread out round the diffraction circle because the cellulose microfibrils wander slightly about the mean angle, so the X-rays see a narrow distribution of microfibril angle. It is assumed that this produces a spread of intensity about the mean angle that is described by a normal Gaussian distribution. So for a cell wall of length ΔL_n the azimuthal distribution of diffracted intensity ΔI_n is given by

$$\Delta I_n = \Delta L_n \exp\left[-1/2\left\{\left(\varphi - \varphi_{ij}\right)/\sigma_\varphi\right\}^2\right] \quad (13)$$

where φ_{ij} is the calculated position of the diffraction spot given by the appropriate equation of the set 7–12, and σ_φ is the standard deviation of the normal distribution.

The intensity distributions on the right and on the left sides of the polar line were calculated separately. A spreadsheet was set-up to perform such calculations. A column listed the 180 values of the cell wall orientations α relative to the incident X-ray beam. The corresponding values of the azimuth angle φ_{1R} for the 1R diffractions from f1 were calculated in an adjacent column using equation 7. The individual cell wall lengths were listed in the next column. A further set of 81 columns covering azimuth angles from –40° to + 40° gave 180 rows along which the distribution of intensity for each diffraction spot was calculated from Eq. 13. The sum of the intensities in each column gave the azimuthal distribution of the total intensity generated by fibril f1. A second spreadsheet gave the corresponding total intensity for diffraction 2R from fibril f2. The sum of the totals for the two fibrils gave the total intensity distribution in the section of the (002) circle to the right of the polar axis. The calculations were performed in a similar fashion to determine the total intensity distribution to the left of the polar axis.

The calculations were repeated for the other seven specimens. In these cases the X-ray beam, which was directed normal to the wider face of the specimen, lay at an angle β to the normal to the radial plane. The orientation of the individual 1° set of cell walls in Fig. 2 is given by the angle θ, which is measured relative to the radial plane. So, in an exposure in which the X-ray beam is directed at an angle β to the radial plane normal, the angle of incidence to a particular cell wall is

$$\alpha = (\beta + \theta) \quad (14)$$

For each calculation, the microfibril angle M and the standard deviation of the scattered intensity from a single fibril σ_φ are adjustable parameters. The values for a particular specimen were obtained by adjusting M and σ_φ to give the best fit to the measured intensity distribution.

Comparison of the measured and the calculated intensity distributions

Figure 7 displays the experimental intensity distributions and the calculated values fitted to them for the eight specimens. The achieved fits are seen to be good. The right hand and the left hand intensity distributions are not similar, apart from the particular case of $\beta = 0°$. Hence, fitted values of M and σ_φ were obtained separately from the right hand and the left hand distributions. The resulting values are listed in Table 1.

The fitted values show a good consistency between the different specimens and between values derived from the left and right hand peaks of a specimen. There is a slight indication that the values of M are smaller for lower values of α. This could imply that the cell walls centred around the radial direction have a lower microfibril angle than those around the transverse direction.

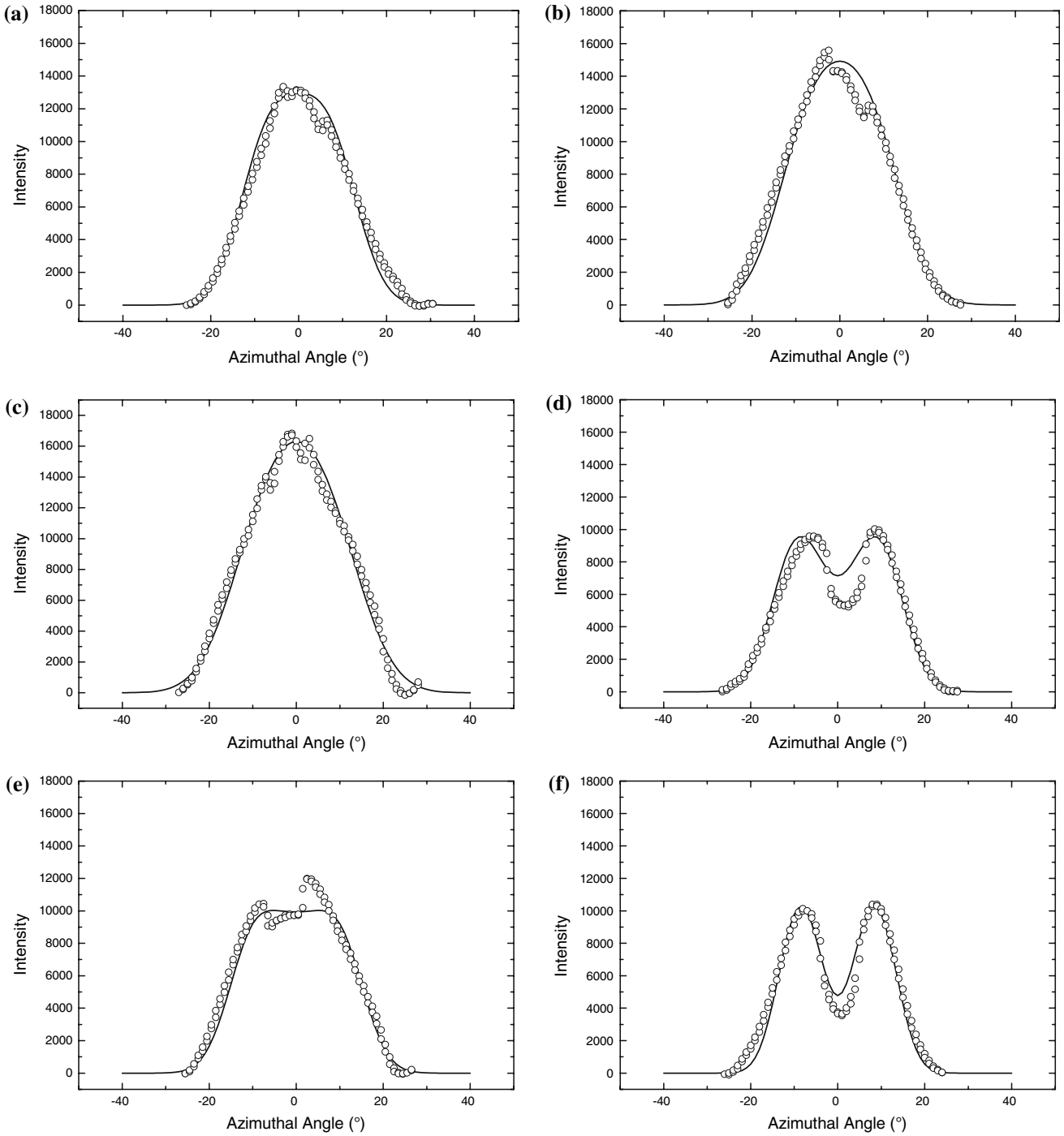

Fig. 7 Curves for the calculated azimuthal distribution of intensity fitted to the measured intensity distribution. (**a**) Right-hand sector, $\beta = 0°$, $M = 9°$, $\sigma_\varphi = 6°$; (**b**) Left-hand sector, $\beta = 0°$, $M = 9°$, $\sigma_\varphi = 7°$; (**c**) Right-hand sector, $\beta = 12°$, $M = 9°$, $\sigma_\varphi = 8°$; (**d**) Left-hand sector, $\beta = 12°$, $M = 12°$, $\sigma_\varphi = 5°$; (**e**) Right-hand sector, $\beta = 22°$, $M = 11°$, $\sigma_\varphi = 6°$; (**f**) Left-hand sector, $\beta = 22°$, $M = 12°$, $\sigma_\varphi = 4°$; (**g**) Right-hand sector, $\beta = 37°$, $M = 12°$, $\sigma_\varphi = 5°$; (**h**) Left-hand sector, $\beta = 37°$, $M = 13°$, $\sigma_\varphi = 4°$; (**i**) Right-hand sector, $\beta = 44°$, $M = 13°$, $\sigma_\varphi = 4°$; (**j**) Left-hand sector, $\beta = 44°$, $M = 14°$, $\sigma_\varphi = 4°$; (**k**) Right-hand sector, $\beta = 50°$, $M = 13°$, $\sigma_\varphi = 4°$; (**l**) Left-hand sector, $\beta = 50°$, $M = 13°$, $\sigma_\varphi = 4°$; (**m**) Right-hand sector, $\beta = 53°$, $M = 12°$, $\sigma_\varphi = 5°$; (**n**) Left-hand sector, $\beta = 53°$, $M = 12°$, $\sigma_\varphi = 5°$; (**o**) Right-hand sector, $\beta = 63°$, $M = 12°$, $\sigma_\varphi = 4°$; (**p**) Left-hand sector, $\beta = 63°$, $M = 11°$, $\sigma_\varphi = 4°$

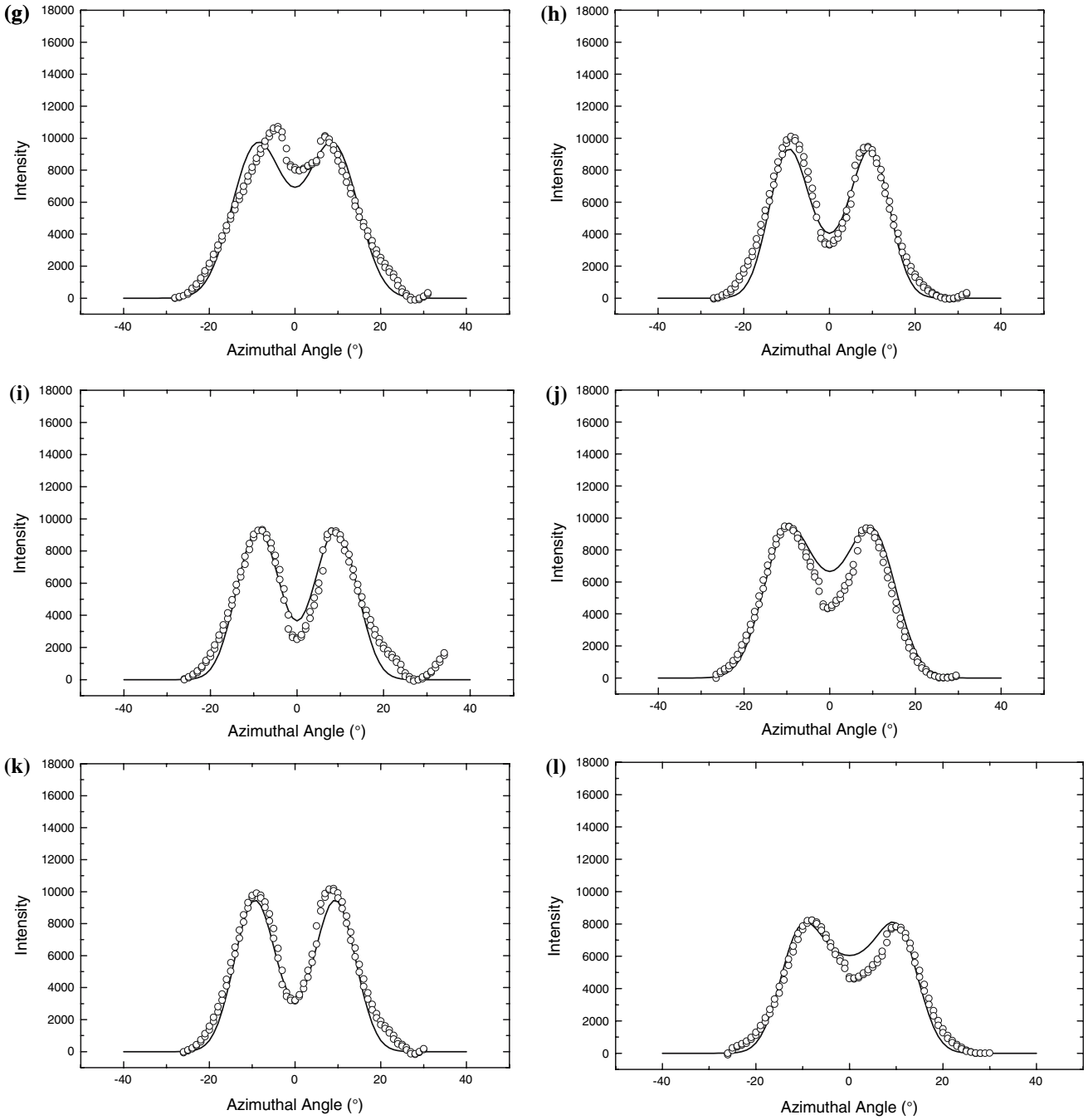

Fig. 7 continued

Comparison between the azimuthal intensity distribution calculated from the real cell wall structure and that for an assembly of square cells

Figure 8 presents a comparison between the azimuthal distribution of scattered intensity calculated from the real cell wall arrangement and that for an assembly of square cells for $\beta = 0°$, 22° and 44°. The assumed values of M and σ_φ are those determined from the fits of Fig. 7a, 7e and 7i and the pairs of curves are scaled for the peak intensities to be equal.

The intensity distributions will always be symmetrical about the equatorial line, provided that the microfibril angles are identical for the two sets of fibrils in a cell wall. The intensity distributions will be symmetrical about the polar line if the X-ray beam lies along a line of symmetry of the cell structure. For square cells this will be the case for $\beta = 0°$ and for $\beta = 45°$. It is evident from Fig. 8 that the

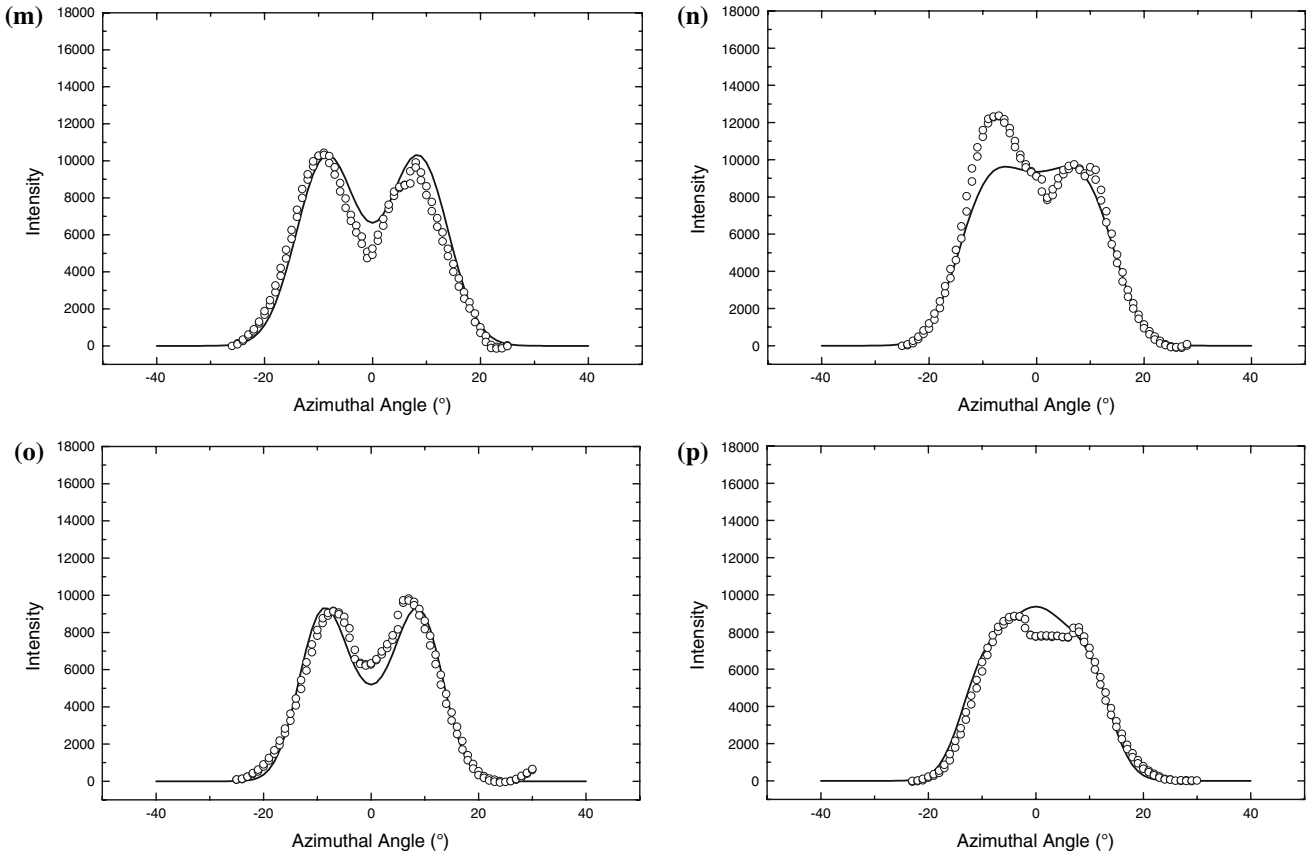

Fig. 7 continued

Table 1 Values of the microfibril angle M and the standard deviation of the intensity distribution for a single fibril σ_φ derived by fitting the calculated peaks to the measured peaks. Data are obtained from both the right hand and the left hand peaks for a range of measurements covering angle of incidence of the X-ray beam β from 0 to 63°

β(°)	Left-hand peaks		Right-hand peaks	
	M(°)	σ_φ(°)	M(°)	σ_φ(°)
0	9	7	9	6
12	12	5	9	8
22	12	4	11	6
37	13	4	12	5
44	14	4	13	4
50	13	4	13	4
53	12	6	12	5
63	11	4	12	4

right- and the left-hand intensity distributions are equal for $\beta = 0°$ and closely equal for $\beta = 44°$ which is close to the value of $\beta = 45°$ for which the equality is exact. For $\beta = 22°$ in Fig. 8 the distributions are distinctly different, as would be expected from the asymmetry of the cell wall arrangements.

The intensity distributions for the real cell wall structure show close equality between the right- and the left-hand distributions for $\beta = 0°$. It is evident from Fig. 2 that the cell wall structure is closely symmetrical about $\theta = 0°$, so that equality is expected. In contrast the right- and left-hand intensity distributions for $\beta = 44°$ in Fig 8 are not equal. This arises because, referring to Fig. 2, the wall structure is asymmetrical about $\theta = 44°$. On one side of the line lie radial cell walls and on the other lie transverse walls and the ratio of radial wall length to transverse wall length is about 1.8. This is the source of the asymmetry. As with the square cells the right- and left-handed distributions for $\beta = 22°$ are markedly asymmetrical.

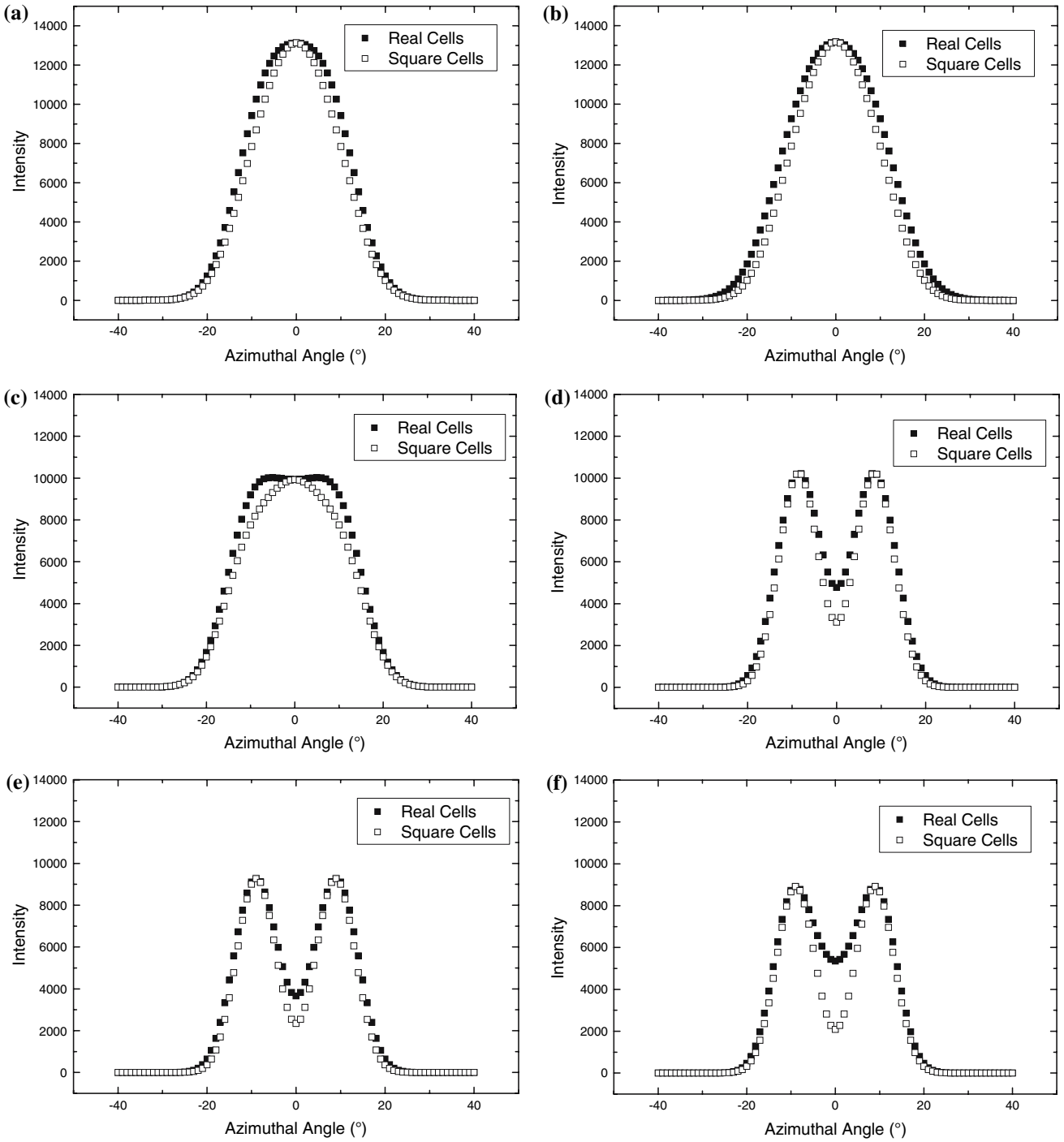

Fig. 8 A comparison between the azimuthal distribution of diffracted intensity calculated from the real cell wall geometry and that calculated for a square cell population. The peak heights have been scaled to be equal. (**a**) $\beta = 0°$, Right-hand sector; (**b**) $\beta = 0°$, Left-hand sector; (**c**) $\beta = 22°$, Right-hand sector; (**d**) $\beta = 22°$, Left-hand sector; (**e**) $\beta = 44°$, Right-hand sector; (**f**) $\beta = 44°$, Left-hand sector

A striking feature of a comparison between the pairs of data in Fig 8 is that the extreme flanks of the real and the square cell curves are very close. This feature has special implications for the curves for $\beta = 0°$ which are commonly used to determine the microfibril angle using the Meylan T parameter [2]. $2T$ is the angular separation between the points of intersection of the tangents to the outer flanks of the intensity distribution and the zero intensity axis. Cave has shown that for square cells irradiated with the X-ray beam normal to one set of cell boundaries [1]

$$T = M + 2\sigma_\varphi \tag{15}$$

where σ_φ is the standard deviation of the intensity distribution from a single fibril. The extreme flanks of all the curves for $\beta = 0°$ will derive from cell walls whose normals are parallel to the incident X-rays. These will be radial walls, and the azimuth angle for the peak intensity will be equal to the microfibril angle. The transverse walls will generate intensity near $\varphi = 0°$ and will not contribute to the intensity in the flank region. So the flank of the intensity curve will be half of a Gaussian distribution of intensity with a maximum at $\varphi = M$ and a standard deviation of σ_φ. It is a feature of the Gaussian curve that tangents to the flanks of the curve cut the axis at a distance of $2\sigma_\varphi$ from the peak value. This is the basis of Cave's relationship [1].

Normally Eq. 15 is not used to determine M because σ_φ is undetermined. Meylan proposed an alternative relation [2]

$$M = KT \tag{16}$$

where K was determined by measuring the micro-fibril angle directly by optical examination of iodine-stained specimens. By this means he found that $K = 0.6$.

We can say, using Eqs. 15 and 16, that

$$K = \frac{M}{M + 2\sigma_\varphi} \tag{17}$$

Since the technique now described yields values for both M and σ_φ it is possible to test if the square cell relation (Eq. 15) can be used to derive a valid value for the micro-fibril angle from the calculated intensity for the real cell structure. Figures 7a and 7b are the intensity curves for the right-hand and the left-hand sectors measured with the X-ray beam directed normal to the radial plane. Values of T obtained by drawing tangents to the calculated intensity curves give values of M listed in Table 2.

The agreement between these two pairs of micro-fibril angles implies that the flanks of the intensity distribution for the real cell structure derive predominantly from that part of the cell wall population which lies close to the radial direction. This conclusion is reinforced by the fact that tangents drawn to the flanks of the intensity curves for square cells and for real cells in Fig. 7a and 7b intersect the zero intensity line at the same point.

Table 2 Values of T derived by drawing tangents to the calculated intensity curves and subsequent values of M derived from Eq. 15

Side of curve	T(°)	σ_φ(°)	M(°)	M via curve fitting (°)
Left-hand	21	6	9	9
Right-hand	22	7	8	9

The conclusion from this analysis is that the Meylan and Cave relations (Eqs. 15 and 16) can be used to derive the microfibril angle from the $\beta = 0°$ intensity distribution for either square cell populations or for more random cell wall structures. However, the problem with the application of this method is that it is necessary to know the standard deviation of the single fibril intensity distribution.

Another method for extracting a value for the microfibril angle is to measure the azimuth angle for peak intensity from a specimen irradiated with $\beta = 45°$. For square cells this angle, φ_{45}, is related to the microfibril angle (M) by

$$M = \arctan\left(\sqrt{2}\tan(\varphi_{45})\right) \tag{18}$$

The data in Figs. 7 and 8 for $\beta = 44°$ are sufficiently close to $\beta = 45°$ to be used for a valid comparison. It is evident from Figs. 8e and 8f that the calculated azimuth angles for peak intensity for square cells and for the real cell structure are equal at $\varphi_{44} = 9°$. If this value is put into Eq. 18 it gives a value of $M = 12.6°$. The measured curves for $\beta = 44°$ in Fig. 7i and 7j also show peaks at azimuth angles of 9°. The values of the microfibril angle obtained by fitting the measured curves to the calculated intensities are 13° and 14° for the two sets of data. These are close to the value of 12.6° obtained by using Eq. 18.

The conclusion from these data is that values of the microfibril angle, adequate for many purposes, can most conveniently be derived by measuring the azimuth angle at the peak intensity for a specimen irradiated with the X-ray beam at 45° to the radial plane. The value of M is then calculated using the relation for square cells given by Eq. 18. An advantage of this method is that it is not necessary to establish the standard deviation of the single fibril intensity. It is therefore recommended as the simplest and quickest way of obtaining values for the micro-fibril angle using X-ray scattering.

Conclusion

Soundly-based values of the microfibril angle in softwood have been derived using the distribution of length and orientation of about 1000 cell walls obtained by quantitative image analysis. The azimuthal distribution of the (002) diffracted intensity was calculated from this cell wall geometry by summing the diffracted intensity from all the individual cell walls. This procedure was carried out for eight different values of the angle of incidence of the X-rays. The calculated curves were fitted to the measured intensity distribution by adjusting the values of the two parameters M and σ_φ.

The greatest differences between the calculated intensity distributions for the real and an assumed square cell population were found to exist around zero azimuth angle. The extreme flanks of the distribution were more similar. One consequence of this is that the three values of the Meylan parameter T derived from (i) the real cell structure, (ii) an assumed square cell structure and (iii) the measured intensity distribution were similar for specimens irradiated normal to the radial planes. Values of the microfibril angle derived from the T value of the experimental curves were in good accord with those derived from fitting the measured and calculated curves. This comparison is possible because the present analysis yielded values for σ_{φ}. In the absence of this information the Meylan method carries uncertainty.

It has been demonstrated that the azimuthal angle (φ_{45}) for the peak intensity from specimens irradiated at 45° to the radial plane is the same for the calculated intensities from both the real cell structure and for square cells. This establishes that a value for the microfibril angle that is adequate for many purposes may be obtained by measuring φ_{45} and calculating the value of M from the relation for square cells. The advantage of this procedure is that it does not require a value for σ_{φ} and is recommended as a quick and simple method for the measurement of micro-fibril angle.

Acknowledgements The authors are grateful to the CCLRC for the award of beamtime at the Daresbury Synchrotron (Station 14.1)

References

1. Cave ID (1966) Forest Prod J 16:37
2. Meylan BA (1967) Forest Prod J 17:51
3. Stuart SA, Evans R (1995) Appita J 48:197
4. Evans R (1999) Appita J 52:283
5. Cave ID (1997a) Wood Sci Technol 31:225
6. Cave ID (1997b) Wood Sci Technol 31:143
7. Müller M., Czihak C, Vogl G, Fratzl P, Schober H, Riekel C (1998) Macromol 31:3953
8. Reiterer A, Jakob HF, Stanzl-Tschegg SE, Fratzl P (1998) Wood Sci Technol 32:335
9. Keckes J, Burgert I, Fruhmann K, Müller M, Kolln K, Hamilton M, Burghammer M, Roth SV, Stanzl-Tschegg S, Fratzl P (2003) Nature Mat 2:810
10. Kolln K, Grotkopp I, Burghammer M, Roth SV, Funari SS, Dommach M, Muller M (2005) J Sync Rad 12:739
11. Barnett JR, Bonham VA (2004) Biol Rev 79:461
12. Entwistle KM, Eichhorn SJ, Navaranjan N (2005) J Appl Cryst 38:505
13. Entwistle KM, Navaranjan N (2001) J Mater Sci 36:3855
14. Hammersley AP, Riekel C (1989) Synch Rad News 2:24
15. Hammersley AP (1997) ESRF Internal Report, ESRF97HA02T. Fit2D: an introduction and overview
16. Marquardt DW (1963) J Soc Ind Appl Math 11:431
17. Entwistle KM, Terrill NJ (2000) J Mater Sci 35:1675